REPORT DOCUMENTATION PAGE

1. REPORT DATE (DD-MM-YYYY) 09-01-2008	2. REPORT TYPE Journal Article	3. DATES COVERED (From - To)

4. TITLE AND SUBTITLE

Structural Investigation of Fluoridated POSS Cages Using Ion Mobility Mass Spectrometry and Molecular Mechanics (Preprint)

5a. CONTRACT NUMBER

5b. GRANT NUMBER

5c. PROGRAM ELEMENT NUMBER

6. AUTHOR(S)
Dena J. Bodzin & Stanley E. Anderson (Westmont College); Timothy S. Haddad (ERC); Jerry A. Boatz (AFRL/RZSP); Joseph M. Mabry (AFRL/RZSM); Connie Mitchell & Michael T. Bowers (USC)

5d. PROJECT NUMBER
23030521

5e. TASK NUMBER

5f. WORK UNIT NUMBER

7. PERFORMING ORGANIZATION NAME(S) AND ADDRESS(ES)

AFRL/RZSM
9 Antares Road
Edwards AFB CA 93524-7401

8. PERFORMING ORGANIZATION REPORT NUMBER

AFRL-RZ-ED-JA-2008-013

9. SPONSORING / MONITORING AGENCY NAME(S) AND ADDRESS(ES)

Air Force Research Laboratory (AFMC)
AFRL/RZS
5 Pollux Drive
Edwards AFB CA 93524-7048

10. SPONSOR/MONITOR'S ACRONYM(S)

11. SPONSOR/MONITOR'S NUMBER(S)
AFRL-RZ-ED-JA-2008-013

12. DISTRIBUTION / AVAILABILITY STATEMENT

Approved for public release; distribution unlimited (PA #08063A)

13. SUPPLEMENTARY NOTES
For publication in the ACS Journal, Chemistry of Materials.

14. ABSTRACT
Ion mobility and molecular modeling methods were used to investigate the gas phase conformational properties of Polyhedral Oligomeric Silsesquioxane (POSS) fluoride salts, where the fluoride is encapsulated within the POSS cage. Theoretical calculations demonstrate that the binding energy of fluoride to the interior of the POSS cage ranges from 70 to 270 kcal/mol as a function of substituent. Sodiated positive ions of the form $HF@R_8T_8Na^+$ ($T = SiO_{3/2}$, R = styrenyl, phenyl, and vinyl) were examined by MALDI; ESI was used to study the negative ions $F^-@R_8T_8$ (R = styrenyl, phenyl, vinyl, trifluoropropyl, and nonafluorohexyl). The ion mobilities of these species were measured and used to calculate collision cross sections. These cross sections were compared to X-ray crystal structures and theoretical cross sections obtained from molecular mechanics and dynamics calculations. Experimental cross sections were consistent with all of the known X-ray crystal structures (styrenyl, vinyl and phenyl POSS species). The experimental cross sections also agreed with the calculated cross sections for each monomer species. Due to the compact nature of the POSS monomer cages, each sample had only one stable conformation, and only one low-energy family of structures was found for each set of sample calculations.

15. SUBJECT TERMS

16. SECURITY CLASSIFICATION OF:			17. LIMITATION OF ABSTRACT	18. NUMBER OF PAGES	19a. NAME OF RESPONSIBLE PERSON Dr. Joseph M. Mabry
a. REPORT **Unclassified**	b. ABSTRACT **Unclassified**	c. THIS PAGE **Unclassified**	SAR	34	19b. TELEPHONE NUMBER (include area code) N/A

Structural Investigation of Fluoridated POSS Cages Using Ion Mobility Mass Spectrometry and Molecular Mechanics

Dena J. Bodzin, Stanley E. Anderson[a], Timothy S. Haddad[b], Jerry A. Boatz[c], Joseph M. Mabry[c], Connie Mitchell and Michael T. Bowers*

Department of Chemistry & Biochemistry, University of California, Santa Barbara, CA 93106

[a]Department of Chemistry, Westmont College, Santa Barbara, CA 93108

[b]ERC Inc., [c]Air Force Research Laboratory, 10 East Saturn Boulevard, Building 8451, Edwards AFB, CA 93524-7680

RECEIVED DATE

TITLE RUNNING HEAD   Structural Investigation of Fluoridated POSS Cages Using Ion Mobility Mass Spectrometry and Molecular Mechanics

CORRESPONDING AUTHOR FOOTNOTE

* Corresponding author: Phone: 805-893-2893. Email: bowers@chem.ucsb.edu

Abstract

Ion mobility and molecular modeling methods were used to investigate the gas phase conformational properties of Polyhedral Oligomeric Silsesquioxane (POSS) fluoride salts, where the fluoride is encapsulated within the POSS cage. Theoretical calculations demonstrate that the binding energy of fluoride to the interior of the POSS cage ranges from 70 to 270 kcal/mol as a function of substituent. Sodiated positive ions of the form $HF@R_8T_8Na^+$ ($T = SiO_{3/2}$, R = styrenyl, phenyl, and vinyl) were examined by MALDI; ESI was used to study the negative ions $F^-@R_8T_8$ (R = styrenyl, phenyl, vinyl, trifluoropropyl, and nonafluorohexyl). The ion mobilities of these species were measured and used to calculate collision cross sections. These cross sections were compared to X-ray crystal structures and theoretical cross sections obtained from molecular mechanics and dynamics calculations. Experimental cross sections were consistent with all of the known X-ray crystal structures (styrenyl, vinyl and phenyl POSS species). The experimental cross sections also agreed with the calculated cross sections for each monomer species. Due to the compact nature of the POSS monomer cages, each sample had only one stable conformation, and only one low-energy family of structures was found for each set of sample calculations.

KEYWORDS POSS, Polyhedral oligomeric silsesquioxane (POSS), POSS siloxane, ion mobility, hybrid inorganic/organic

Introduction

In the field of materials science, much current research focuses on the ability to enhance properties of materials for increased performance and environmental robustness. One approach to developing better materials is to create inorganic/organic composite materials in which inorganic building blocks are incorporated into organic polymers. Polyhedral Oligomeric Silsesquioxanes (POSS) are one type of hybrid inorganic/organic material of the form $(RSiO_{3/2})_n$, abbreviated R_nT_n, where organic substituents (R_n) are attached to a silicon-oxygen cage.[1] The most common POSS cage is the R_8T_8, a molecule with a cubic array of silicon atoms and bridging oxygen atoms with eight R groups at the vertexes of the cube; other cages with well-defined geometries include n = 6, 10, 12, 14, 16 and 18.[2, 3] When these Si-O cage structures are incorporated into organic polymers, exciting possibilities for the development of new materials are often realized,[4-9] with properties superior to the original organic polymer. For example, the low surface energy properties of fluorinated POSS compounds have been used to augment both fluorinated and non-fluorinated polymers.[10-13]

Many POSS monomers have been successfully characterized using MALDI techniques[14-16] in conjunction with ion mobility mass spectrometry.[17-19] The POSS cages have good ionization efficiencies due to electronegative atoms or π-electron density in the R-groups and readily bind protons or alkali metal cations to give positive ions. Fragmentation of the cage may occur at high laser powers, but this has not been enough of a factor to prevent observation of a strong molecular ion peak. Bulky alkyl R-groups seem to inhibit the formation of positive ions and signals for such POSS species are rarely seen.

Extending the study of POSS systems from monomers to polymers and oligomers relies on our ability to generate large ions in the gas phase without fragmentation. Ion mobility studies coupled with molecular dynamics modeling of other types of large polymers,[20-23] including DNA[24, 25] and proteins,[26] have shown great success. However, there are only a few papers reporting mass

spectra of POSS polymers.[27] Larger POSS oligomers may have lower ionization efficiencies than the monomers, most likely due to decreased charge density, because POSS cages are efficient in delocalizing electron density. The oligomers may also have an increased tendency to fragment. Our group has been successful in characterizing two oligomer systems, the POSS propylmethacrylates and siloxanes, but only up to systems with three POSS cages.[28, 29] The intensity of the molecular ion peak generally decreases with increasing oligomer size to the point that it becomes impossible to obtain ion mobility data. To facilitate the observation of higher POSS oligomers by mass spectrometric methods, it has been necessary to develop new strategies that will enhance the ionization efficiency of these compounds.
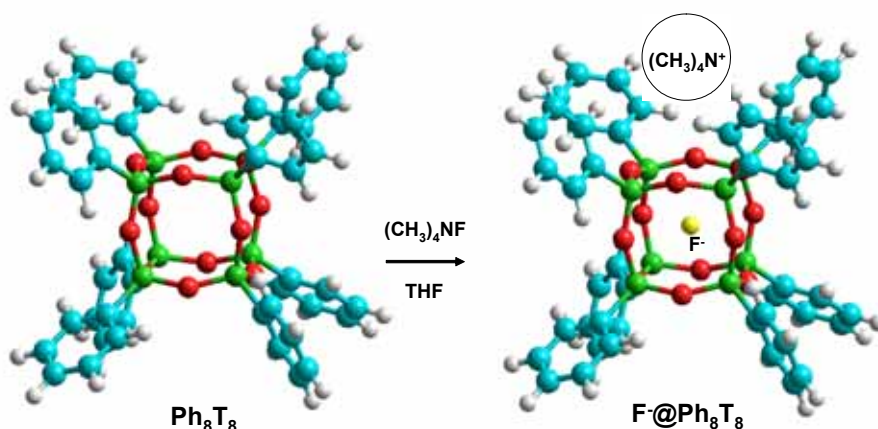

Figure 1. Synthesis and structure of F⁻@Ph$_8$T$_8$.

Methods for increasing the ionization efficiency of these POSS materials must begin with the synthesis of these molecules. Both acid- and base-catalyzed methods have proved fruitful in creating many new molecules with a variety of R-groups, but often in relatively low yield.[1] Bassindale and co-workers[30, 31] have succeeded not only in increasing the POSS yield dramatically by using tetrabutylammonium fluoride (TBAF) under scarce-water hydrolysis conditions as a catalyst, but in synthesizing a new class of POSS materials in which a fluoride ion is trapped in the center of a POSS cage, denoted F⁻@R$_8$T$_8$ (see Figure 1). They have demonstrated incorporation of fluoride into the cage using NMR chemical shifts, and more importantly, have obtained crystal structures of POSS monomers where R = vinyl, phenyl, and p-tolyl, where the F⁻ ion is clearly in the center of the cage. The fluoride ion results in only a very slight change in the Si-O distances and

cage bond angles from structures where the central fluoride is absent.

The stability of the fluoridated POSS cage depends on the nature of the organic capping groups. Theory[32-35] has shown that when R is a highly delocalized π-system, as opposed to an electron donating alkyl R group, the HOMO and LUMO are outside of the cage primarily centered on the organic ligands. This leaves the center of the cage with an effective positive charge, stabilizing the fluoride structure. Conversely, when R is an electron donating alkyl group, the HOMO is associated primarily with the cage atoms, resulting in a net negative charge on the cage. This would destabilize the fluoride structure. In fact, attempts to synthesize fluoride salts of alkyl-substituted POSS have failed.

Each of the successfully synthesized fluoridated POSS species has been characterized by ion mobility mass spectrometry and molecular modeling techniques. The capping groups that yielded stable fluoridated structures include phenyl, vinyl, styenyl, trifluoropropyl, nonafluorohexyl, and a mixture of isobutyl and styryl ligands. Each of these R groups demonstrates electron-withdrawing properties, accounting for the stabilization of the interior fluoride ion as predicted.

Incorporation of the fluoride into these monomers suggests a tool to study higher molecular weight oligomers. If even a single POSS cage within the molecule were able to incorporate fluoride, this would increase the ionization efficiency of the oligomer. If several of the POSS units in the oligomer incorporated fluoride ions, it would greatly increase ionization efficiency as well as reduce the mass to charge ratio of the ion, resulting in a sample that would be easier to study by mass spectrometric methods. Here we describe in detail our initial studies of F^- and HF bound in the interior of the POSS cage and demonstrate the effectiveness of IM-MS for studying these systems.

Materials and Methods

General POSS Synthesis Procedures

POSS materials used for this study were either purchased from Hybrid Plastics (Methyl$_8$T$_8$, Vinyl$_8$T$_8$, Phenyl$_8$T$_8$, isoButyl$_8$T$_8$, CycloHexyl$_8$T$_8$) or else synthesized according to the literature procedures[36-41] (Ethyl$_8$T$_8$, TrifluoroPropyl$_8$T$_8$, NonafluoroHexyl$_8$T$_8$, TridecafluoroOctyl$_8$T$_8$, Styrenyl$_8$T$_8$, isoButyl$_7$(Styryl)T$_8$). Tetramethylammonium fluoride (TMAF) was purchased from Aldrich and used as received. Tetrahydrofuran (THF) was dried through an activated alumina column,[42] freeze-pump-thawed three times to remove any oxygen, and stored under an inert nitrogen atmosphere in a dry box.

Synthesis of Fluoridated POSS Salts

All syntheses were carried out in the same manner. 200 mg of the parent POSS cage along with 1 molar equivalent of TMAF was placed into 10 mL of anhydrous THF and stirred for 16 hours. A sample synthesis is as follows: In a 25 mL flask 200 mg (0.194 mmole) of Phenyl$_8$T$_8$ and 18 mg (0.19 mmole) of TMAF were suspended in THF and stirred for 16 hours. The cloudy suspension became translucent after a few hours. This was filtered through Celite and the solvent was removed under vacuum to give a virtually quantitative yield of encapsulated fluoride salt. This synthesis worked well for POSS cages substituted with electron withdrawing groups: vinyl (Si-CH=CH$_2$), phenyl (Si-C$_6$H$_5$), styrenyl (Si-CH=CHC$_6$H$_5$), trifluoropropyl (Si-CH$_2$CH$_2$CF$_3$), nonafluorohexyl (Si-CH$_2$CH$_2$CF$_2$CF$_2$CF$_2$CF$_3$) and tridecafluorooctyl (Si-CH$_2$CH$_2$CF$_2$CF$_2$CF$_2$CF$_2$CF$_2$CF$_3$). It failed to produce any fluoridated product for cages substituted with the electron donating groups, methyl, ethyl, isobutyl or cyclohexyl. In these cases, unreacted starting material was recovered. Complex mixtures of products were obtained from using POSS cages with both types of substituents such as isoButyl$_7$(Styryl)T$_8$. Products were characterized by ^{29}Si and ^{19}F NMR, before and after reaction with TMAF. ^{29}Si and ^{19}F NMR spectra were referenced

to either external tetramethylsilane or $CFCl_3$ at 0 ppm. The ^{19}Si NMR spectra show changes in the environments of the silicon atoms, and the ^{19}F NMR show an additional fluoride present in each sample after reaction with TMAF. The details of this characterization are summarized in the supplemental materials.

Ion Mobility/Mass Spectrometry

High-resolution mass spectra were acquired using a PE Sciex QStar quadrapole/time-of-flight tandem mass spectrometer with a nano-ESI source. Two different home-built instruments were used for the ion mobility mass spectrometry experiments on these compounds. The components and operation of these instruments have been previously published,[28, 29, 43] and the details will not be repeated here. In each case, the instrument can be used to generate a mass spectrum, where a range of m/z is detected, or an arrival time distribution (ATD), where a specific m/z is detected as a function of time.

MALDI

To examine positive ions, a MALDI-TOF equipped with an ion mobility drift cell was used.[28, 29] The matrix was 2,5-dihydroxybenzoic acid (DHB) with THF as the solvent. Approximately 60 μL DHB (100 mg/mL), 40 μL POSS (1 mg/mL), and 8 μL NaI (saturated solution) were mixed and applied to the sample target. A nitrogen laser (λ = 337 nm, 12 mW power) was used to ionize the sample in the ion source. The ions were guided out of the source with 9 kV of extraction voltage, and sent through a 1-m flight tube. The ions were then reflected and redirected to a detector, resulting in a high-resolution mass spectrum of the ions generated at the source. To perform ion mobility measurements, the reflecting lenses were switched off, and the ions continued out of the flight tube to a mass gate. There, mass-selected ions were injected into a 20-cm

glass drift cell filled with ~1.5 Torr of helium gas. The ions drifted through the cell under the influence of a weak electric field, passed through a quadrupole mass filter, and were detected.

ESI

The instrument used to analyze the negative POSS samples was a nano-ESI, also equipped with an ion mobility cell.[43] Approximately 7 μL of POSS solution (~0.1 mg/mL in THF) was loaded into a metalized glass needle. A voltage was applied between the needle and the instrument, spraying the solution out of the needle, through a capillary and into an ion funnel. The ions were then injected into a 4.5 cm drift cell filled with ~5 Torr of helium gas. Again, the ions were pulled through with a weak electric field. After exiting the cell, the ions were mass analyzed by a quadrupole mass filter and detected.

Data Analysis

For each of these instruments, a timing sequence is initiated when the pulse of ions is generated for injection into the drift cell. The time it takes for these ions to reach the detector, t_A, is the sum of the time spend in the drift cell, t_d, and the time spent out of the drift cell, t_o. The amount of time that is required for an ion to drift through a cell filled with helium depends on how many collisions the ion has with the buffer gas, which in turn depends on the effective mobility of the ion. These collisions, along with the electric field across the cell, result in a constant drift velocity v_d

$$v_d = KE = K_o E \frac{760}{p} \frac{T}{273.16} \qquad (1)$$

where K is the mobility of the ion at temperature T and pressure p, and K_o is the reduced mobility. Equation 1 can be rewritten in terms of the arrival time

$$t_A = \frac{l^2}{K_o} \frac{1}{760} \frac{273}{T} \left(\frac{p}{V} \right) + t_o \qquad (2)$$

where l is the cell length, and V is the voltage across the cell. A plot of t_A vs. p/V yields a straight line with a slope proportional to $1/K_o$ and an intercept of t_o. Once K_o is known, it is straightforward to find the cross section σ from Equation 3

$$\sigma = \frac{3q}{16NK_o} \left(\frac{2\pi}{\mu k_b T} \right)^{\frac{1}{2}} \qquad (3)$$

where q is the charge on the ion, N is the number density of the gas in the cell, μ is the ion-He reduced mass, and k_b is Boltzmann's constant.[44]

Theoretical Modeling

We carried out molecular mechanics/molecular dynamics (MM/MD) calculations using the AMBER 7 and 8 suites of programs[45-47] to obtain low-energy structures, and an annealing protocol that utilizes repeated cycles of high temperature heating, cooling and energy minimization. The annealing protocol typically heats structures to 1400 K for 10 ps and then cools exponentially for 30 ps to 50 K before energy minimization. Cations were restrained using a built-in AMBER distance restraint so that they did not "dissociate" at high temperature. At least 100 candidate structures were used to generate a diagnostic graph of calculated cross-sections vs. relative energy. In order to model POSS materials, we developed AMBER parameters for Si from the ab initio calculations of Sun and Rigby[48, 49] that were originally designed to provide force field parameters for polysiloxanes. Our parameter database was updated using recent crystal structure data[30, 50] which give more accurate Si-O and Si-C distances and which reproduce experimental cross-sections. We used HyperChem[35] to build starting structures for AMBER and to visually inspect the calculated minimum energy structures. Charges were calculated by the standard RESP protocol.

A modified projection model[51, 52] was used to calculate accurate cross-sections for systems

with masses below about 1500 amu. For systems above about 1500 amu this method underestimates the true cross-section, due to the occurrence of multiple ion-He encounters during collisions. Between 1500 and 5000 amu a trajectory model is utilized that incorporates a Lennard-Jones interaction portenial.[53] It is our experience that this model can, at times, overestimate the cross-section, but usually gives more reliable values than the projection model in this size range. For larger systems the Lennard-Jones potential is replaced by a hard sphere potential that generally gives reliable results.[54]

Electronic Structure Calculations

Density functional theory (DFT) calculations[55] utilizing the B3LYP hybrid functional[56-58] and the 6-31G* basis set[59-64], denoted as B3LYP/6-31G*, were carried out using the Gaussian 03[65] and GAMESS[66, 67] quantum chemistry software packages The latter program was the primary computational tool because of its ability to run efficiently in parallel using hundreds of processors. The geometry of each species was fully optimized and verified as a local minimum on the ground state potential energy surface via diagonalization of the matrix of energy second derivatives with respect to nuclear coordinates; i.e., the hessian matrix. Selected species were reoptimized using the more flexible 6-311++G(d,p) basis set[63, 68-70] (B3LYP/6-311++G(d,p)). Finally, relative energies were refined via DFT and second order perturbation theory (MP2, also known as MBPT(2)[71-74]) single-point energy calculations using the 6-311++G(2df) basis set[68-70] at the B3LYP/6-31G* geometries, denoted as B3LYP/6-311++G(2df)//B3LYP/6-31G* and MP2/6-311++G(2df)//B3LYP/6-31G*, respectively.

Results and Discussion

The reaction of TMAF with R_8T_8 POSS cages containing eight electron withdrawing groups leads to a quantitative conversion to a salt where the fluoride ion is trapped within the POSS cage (Figure 1). ^{29}Si and ^{19}F NMR spectra of the products are consistent with a single pure compound being formed, and the chemical shifts are comparable to those reported by Bassindale et al for tetrabutylammonium POSS fluoride salts. The reaction is successful for R = phenyl, vinyl, styrenyl, trifluoropropyl, nonafluorohexyl and tridecafluorooctyl POSS derivatives. All attempts to incorporate fluoride into the electron-donating alkyl POSS monomer cages of (ethyl)$_8$T$_8$ (cyclohexyl)$_8$T$_8$ and (i-Butyl)$_8$T$_8$ failed, with only unreacted starting material recovered; no observable signal was found in the ^{19}F NMR spectra. Mass spectra and ion mobility for most of the POSS fluoride salts were obtained and will be discussed in turn. The calculated and experimental cross sections for each negative ion of the form $F^-@R_8T_8$ are given in Table 1, and the equivalent measurements of the sodiated species, $HF@R_8T_8Na^+$, are given in Table 2.

TMAF reactions in the presence of water

If the POSS cages are reacted with TMAF in the presence of water, the cage structure is hydrolyzed and a complex mixture of products is formed in situ. These compounds were characterized by ESI MS. The resulting mass
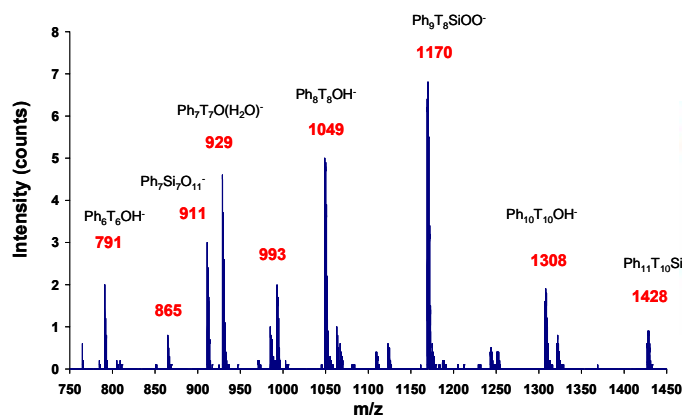

Figure 2. ESI mass spectrum of oxo species derived from Ph_8T_8 and $Ph_{12}T_{12}$.
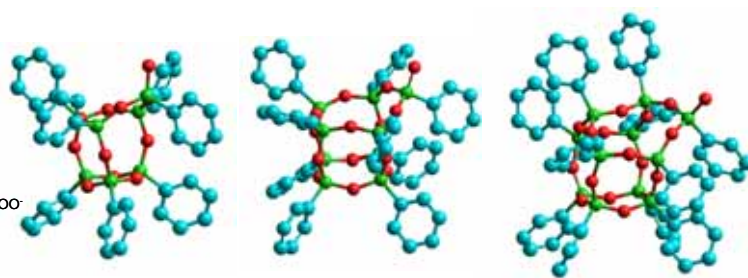
Figure 3. $Ph_7T_7O^-$, $Ph_9T_9O^-$ and $Ph_{11}T_{11}O^-$ structures derived from Ph_8T_8 and $Ph_{12}T_{12}$. Silicon atoms are green, O is red, C atoms are blue, and H atoms are omitted.

11

spectrum is shown for the phenyl species (both Ph_8T_8 and $Ph_{12}T_{12}$ cages) in Figure 2, and equivalent results were seen for the vinyl POSS species. In each case, formation of the oxidized (oxo) species involved complex cage rearrangement. Structures of a few of the resulting species can be seen in Figure 3. The mechanism for formation of these species is unknown, but must involve a preliminary step of either F^- or OH^- atacking an edge of the POSS cage to open it up, followed by insertion of a $R\text{-}SiO_2^-$ fragment and ring closure to reform a larger cage. In order to incorporate fluoride into a POSS cage that remains intact, it is crucial that the reaction take place in an anhydrous environment.

F^-@Phenyl$_8$T$_8$

The synthesis of F^-@Phenyl$_8$T$_8$ from Phenyl$_8$T$_8$ and TMAF yields a well-characterized product. However, the related synthesis of F^- @Phenyl$_7$(ethylnorbornene)T$_8$ gives a less well defined product in which there are chemical shifts indicative of three fluoride environments plus another chemical shift which exactly matches pure F^-@Phenyl$_8$T$_8$. This implies that the fluoride ion causes cage rearrangement to the more stable symmetrically substituted parent. The NMR spectrum for F^-@Phenyl$_8$T$_8$ gives a single F chemical shift consistent with trapped fluoride. A Phenyl$_n$T$_n$ mixture reacted with TMAF gives exclusively the F^-@Phenyl$_8$T$_8$
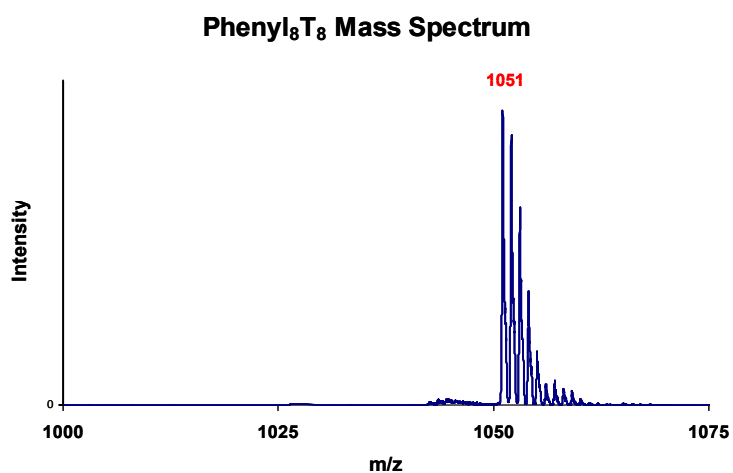

Figure 4. ESI mass spectrum of F^-@Phenyl$_8$T$_8$. The ^{13}C isotope distribution commencing with m/z = 1051 corresponds to the theoretically expected distribution.

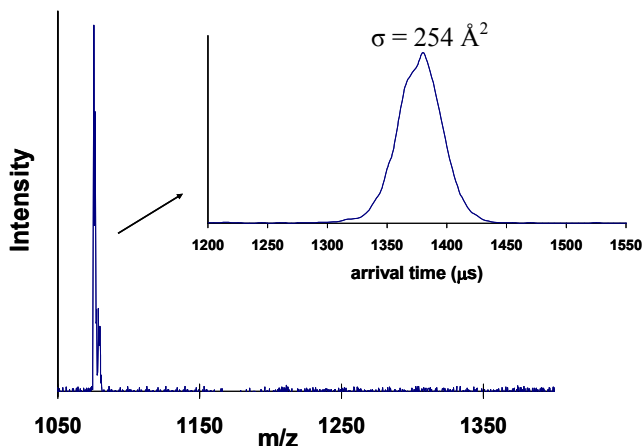**Figure 5.** MALDI mass spectrum and ATD (inset) of HF@Phenyl$_8$T$_8$Na$^+$.

12

product as shown both by NMR and mass spectroscopy.

The high resolution ESI mass spectrum for the F^-@Phenyl$_8$T$_8$ negative ion is given in Figure 4. The multiple peaks commencing at m/z 1051 reveal an isotope distribution which corresponds exactly with the calculated ^{13}C theoretical distribution. A single peak ATD is observed with a width consistent with a single species with an experimental cross-section of 268 Å^2. Molecular modeling predicts a single family of structures with a calculated cross-section of 260 Å^2. The positive ion, HF@Phenyl$_8$T$_8$Na$^+$, was examined by MALDI and also shows a single ATD feature (Fig. 5) with an experimental cross section of 254 Å^2. This compares with a theoretical cross-section of 257 Å^2 for this sodiated species.

F^-@Vinyl$_8$T$_8$

The ESI mass spectrum for the F^-@Vinyl$_n$T$_n$ negative ions where n = 8, 10, 12, and 14 is given in Figure 6. The experimental cross-sections of the fluoride species up to n = 12 (the n = 14 ATD intensity was too small to make arrival time measurements) are given in Table 1 and are in very close agreement with the theoretical values.
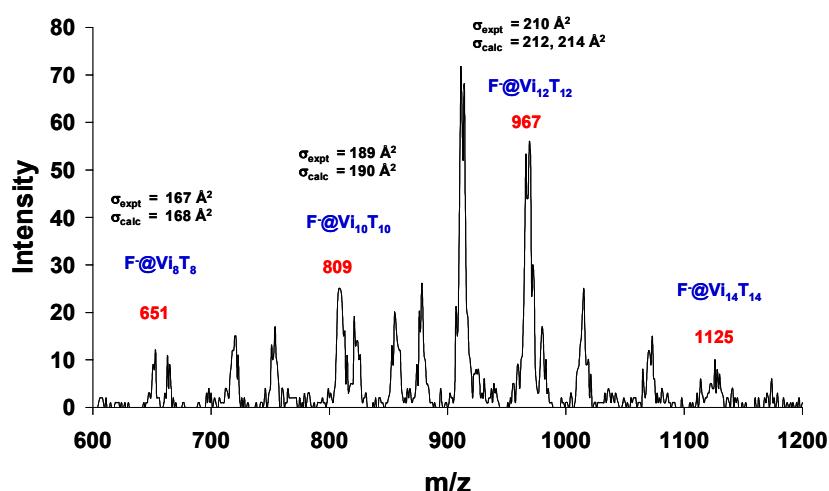

Figure 6. ESI mass spectrum of fluoride species derived from Vi$_8$T$_8$, Vi$_{10}$T$_{10}$, Vi$_{12}$T$_{12}$, and Vi$_{14}$T$_{14}$ mixture.
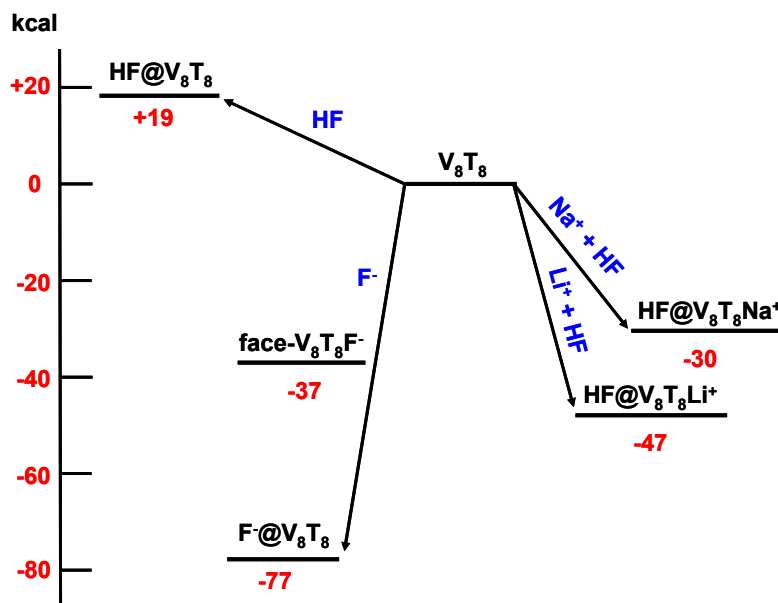

Figure 7. MP2 Stabilization Energies for Vi$_8$T$_8$ Fluoride Monomer Species.

13

Calculations at the B3LYP/6-311++G(2df)//B3LYP/6-31G* and MP2/6-311++G(2df)//B3LYP/6-31G* levels predict the binding energy of the fluoride ion in the V_8T_8 cage to be -63 and -77 kcal/mol, respectively, which is quite large and accounts for the thermodynamic stability of such species. If the fluoride ion were bound on a face of the T_8 cage the binding energy of -37 kcal/mol is still considerable but smaller, explaining the preference for encapsulation. MALDI ionization produces species in the TOF spectrum consistent with the formula $HF@Vi_8T_8M^+$. The matrix adds a proton to the fluoride in $F^-@Vi_8T_8$ giving a neutral HF molecule and binding a M^+ cation. The formation of either the Li^+ or Na^+ cationized species gives binding energies of -47 and -30 kcal/mol, respectively, at the MP2/6-311++G(2df)//B3LYP/6-31G* level. These results are summarized in Table 3 and pictorially in Figure 7.

To test the effect of possible matrix anions forming ion clusters to give the neutral species $HF@Vi_8T_8M_nCl_n$, the binding energies of these clusters are listed in Table 4. M_nCl_n clusters where n = 1, 2, 4 are about 30-50 kcal/mol less stable than the cationized species, but should still be formed. This would reduce the total ion current because of the POSS cages that would exist as neutral species in the gas phase instead of as ions. The effect of cage size (except for T_6) and cation (except for K^+) is minimal on these cluster binding energies, and is not a factor for the R_8T_8 species studied because the positive ions used were consistently Li^+ or Na^+.

$F^-@Styenryl_8T_8$

The MALDI mass spectrum of the Styrenyl$_8$T$_8$ fluoride salt is shown in Figure 8. The mass spectrum corresponds to a sodiated ion in which the fluoride is protonated to give HF, trapped in the POSS cage. The single peak in the ATD gives an
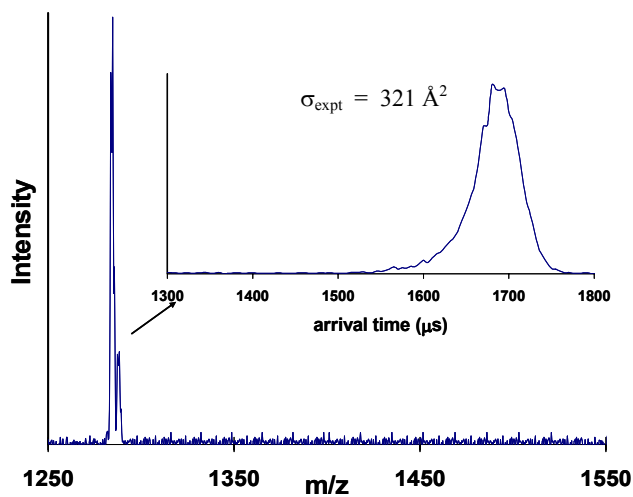

Figure 8. MALDI mass spectrum and ATD (inset) of fluoride species derived from sodiated HF@Styrenyl$_8$T$_8$.

experimental cross-section of 321 Å^2, which corresponds closely to the theoretical value of 325 Å^2. The equivalent negative ion examined by ESI gives experimental and theoretical cross sections of 346 and 343 Å^2, respectively. The positive ion cross sections are consistent with one or two styrenyl groups having isomerized (Fig. 9) from trans to cis to give a structure smaller than the all trans structure (σ_{calc}= 343 Å^2). This explanation is consistent with previous mass spectrometry and ion mobility studies on the sodiated $Styrenyl_8T_8$ species that yielded a complex ATD corresponding to families of paired styrenyl groups and minor features corresponding to "cis impurities."[14, 16] The cis

structure cannot be an artifact of the synthesis, as the change would have been detectable by the NMR characterization, but it may be a result of activation of the double bond in the trans styrenyl group during the MALDI process. The fact that the all-trans species was not observed suggests the single cis isomer is more stable.
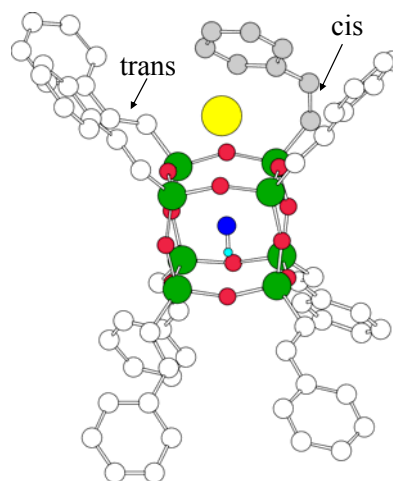
Figure 9. Structure of sodiated $HF@Styrenyl_8T_8$ ion. σ_{exp} = 321 Å^2 and σ_{calc} = 325 Å^2
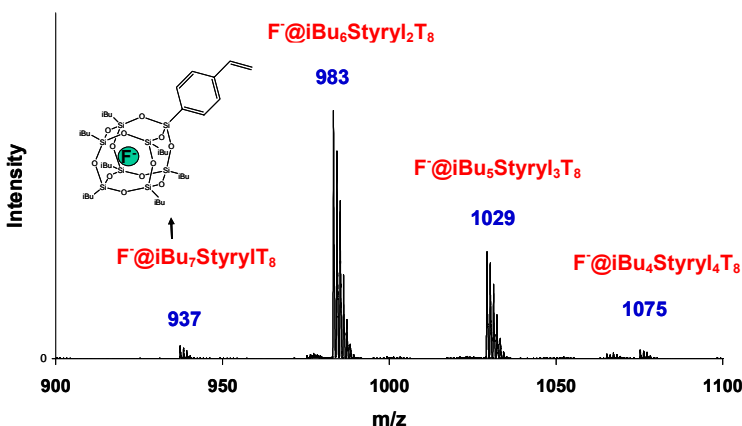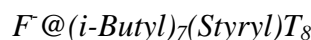
$F^-@(i\text{-}Butyl)_7(Styryl)T_8$

Figure 10. ESI mass spectrum of fluoride species derived from $(i\text{-}Bu)_7(C_6H_5CH=CH_2)_8T_8$. R-group scrambling has occurred.

The ESI mass spectrum for the $F^-@(i\text{-}Butyl)_7(Styryl)T_8$ negative ion and other species related to the parent ion is given in Figure 10. The only reasonable explanation for these additional products is that in the presence of TMAF, the parent structure undergoes complex cage opening and rearrangement which

scrambles the i-butyl and styryl groups. This is consistent with the ^{19}F NMR spectrum which shows at least six environments for the fluoride ion with chemical shifts between -24.5 and -26.3 ppm. Four of these are clearly identifiable in Figure 10. ATDs were measured for the most intense peaks and the cross-sections from experiment and theory are in close agreement and are listed in Table 1.

F⁻@Trifluoropropyl₈T₈

The ESI mass spectrum for the F⁻@Trifluoropropyl₈T₈ species has a single peak at 1211 mass units corresponding to the parent ion. The experimental cross section from the ESI ATD is 251 Å^2, in good agreement with the calculated cross-section of 256 Å^2. Using coordinates from a recent X-ray crystal structure[37a] gives a calculated cross-section of 261 Å^2, slightly larger than what is seen in the gas phase. This difference can be attributed to the way that the trifluoropropyl groups are constrained via non-bonded interactions or packing in the crystal.

A trifluoropropyl group differs from the previous phenyl, vinyl and styrenyl structures described above in that no extended π system is present. However, the CF$_3$ component of this R-
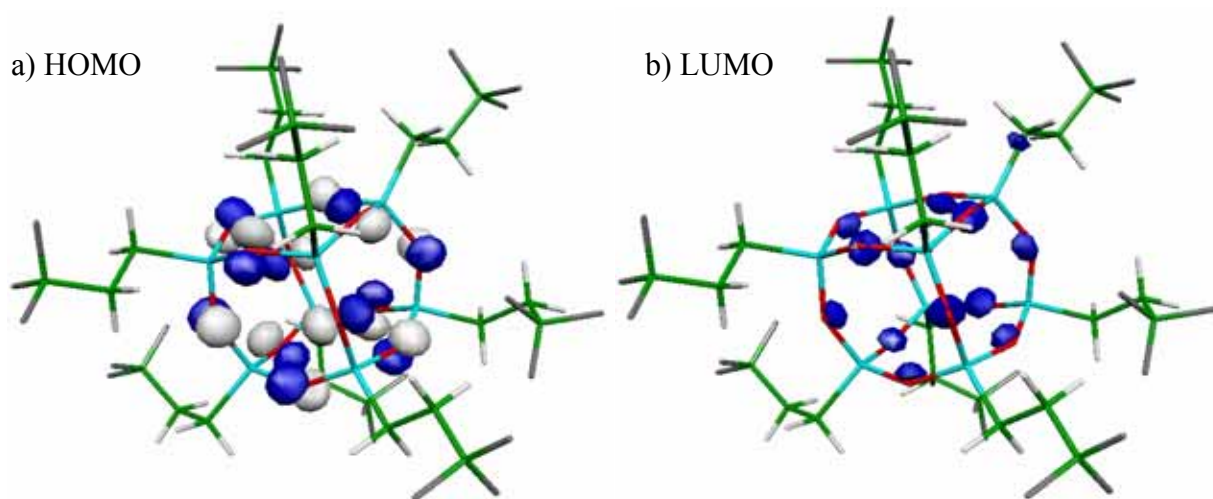
Figure 11. (a) HOMO of $[(CF_3(CH_2)_2]_8T_8$ comprised of cage oxygen lone pairs. (b) LUMO of $[(CF_3(CH_2)_2]_8T_8$ comprised of cage oxygen antibonding σ* orbitals. Frontier orbitals are primarily centered on the R group.

group is strongly electron-withdrawing, which makes the cage more positively charged and thus

facilitates incorporation of a fluoride ion. DFT calculations were used to study the electronic structure of $[CF_3(CH_2)_2]_8T_8$ and $(CF_3)_8T_8$ as well as the fluoridated species. The latter show a large F⁻ binding energy of -171 kcal/mol. The electron densities of the HOMO (molecular orbital 300) and LUMO (molecular orbital 301) are shown in Figure 11. Examination of the frontier orbitals in the vicinity of the HOMO and LUMO has indicated that the orbitals are primarily centered on the $CF_3(CH_2)_2$ groups rather than on the POSS cage. This is similar to the electronic structures of the previous ligands with extended π systems, where the cage has a net positive charge. It is not surprising that POSS cages with similar electronic structures incorporate fluoride in a similar manner to give stable products. In contrast, calculations on a POSS cage capped with methyl groups, $Methyl_8T_8$, show that the electron density is increased on the cage and F⁻@Methyl$_8$T$_8$ is not observed because incorporation of a fluoride ion is unfavorable. This is not a thermodynamic effect, as the binding energy of the fluoride is only slightly less for the methyl compared to the vinyl POSS species (-70 vs -77 kcal/mol, respectively, at the MP2/6-311++G(2df)//B3LYP/6-31G* level). The fact that the fluoridated methyl species cannot be synthesized suggests that a facile kinetics pathway for F⁻ insertion is not accessible, perhaps due to the negative charge on the POSS cage.

R=CH₃	R=CF₃	R=CHCH₂
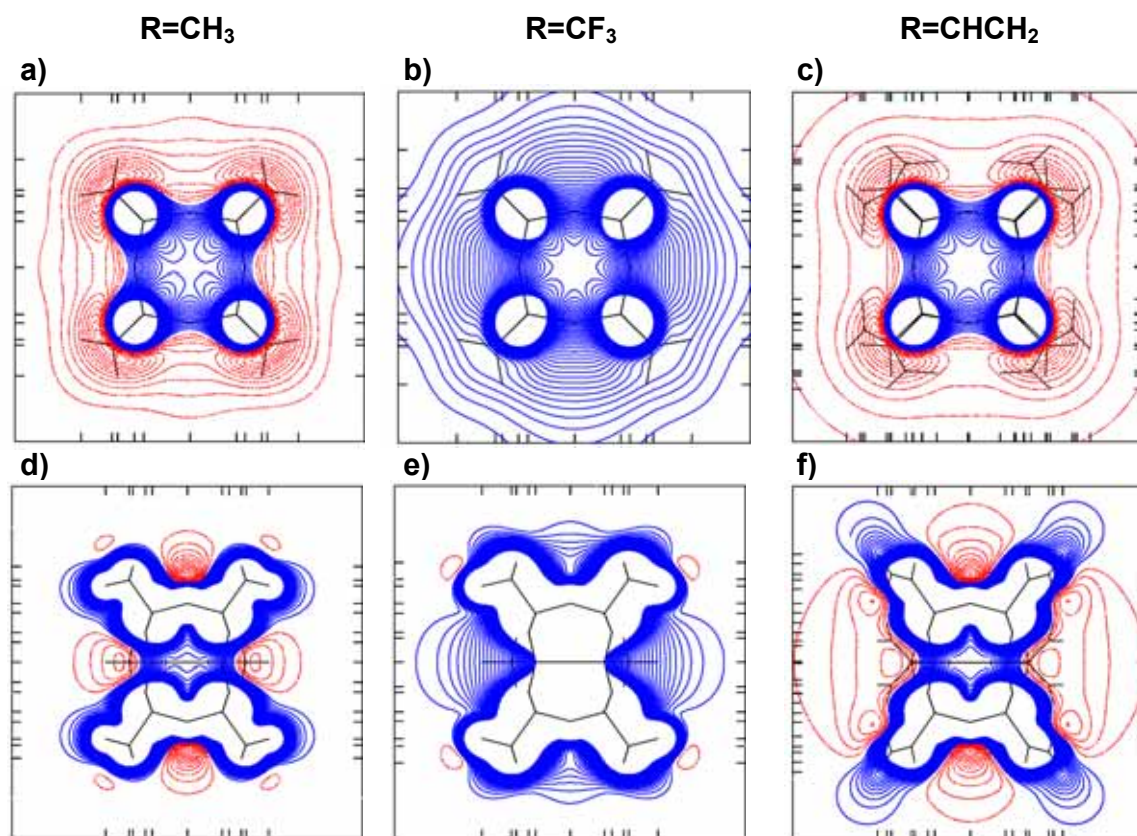
Figure 12. Two-dimensional contour plots of the B3LYP/6-311++G(d,p) molecular electrostatic potentials of R_8T_8 POSS cages; R=CH$_3$, CF$_3$, CHCH$_2$. The plotting plane in panels a-c contains the center of the POSS cage and 4 oxygen atoms, while panels d-f show a diagonal plane through the center of the cage and 4 silicon atoms. The increment between adjacent contours is 2.5 kcal/mol-electron with positive and negative values shown in blue and red, respectively. In panels a-c and d-f, the contours vary from -100.5 to +100.5 and from -80.5 to +80.5 kcal/mol-electron, respectively. The distance along each axis in plots a-c (d-f) is 12 (16) angstroms.

In order to examine the substituent effects on the electronic structure of the T_8 cage, the geometries of T_8R_8, with R=CH$_3$, CH$_2$=CH, and CF$_3$ were reoptimized at a higher level of theory (B3LYP/6-311++G(d,p)), with the resulting molecular electrostatic potential (MEP) plots shown in Figure 12. Positive contours, representing susceptibility to nucleophilic attack, are shown in blue. Negative contours, showing susceptibility to electrophilic attack, are shown in red. The positive contour of the R=CF$_3$ plot shows that this system is particularly susceptible to nucleophilic attack by F$^-$ and is consistent with the large binding energy calculated for both F$^-$@(CF$_3$)$_8$T$_8$ and F$^-$@(CF$_3$CH$_2$CH$_2$)$_8$T$_8$. The difference between the R=CH$_3$ and R=CHCH$_2$ is more subtle and argues for a "kinetic" effect since the binding energies are so similar. The negative contours of R=CH$_3$

18

account for the fact that this molecule does not incorporate F$^-$. The R=CHCH$_2$ plot shows much more diffuse negative contours, probably making attack by F$^-$ more likely in comparison. This interpretation is consistent with the fact that the vinyl species does indeed incorporate fluoride. The vinyl group is apparently efficient in delocalizing electron density away from the cage; the opposite is true for the methyl group. Recent calculations by Kudo and Gordon[75] on the kinetic pathways for POSS cage synthesis highlight the importance of substituents on the silicon atoms for all reaction mechanisms.

F$^-$@Nonafluorohexyl$_8$T$_8$

The ESI mass spectrum for the F$^-$@Nonafluorohexyl$_8$T$_8$ negative ion has a single peak at 2410 mass units corresponding to the parent ion (Fig. 13). The experimental cross section from the ESI ATD is 374 Å^2 compared to the calculated cross-section of
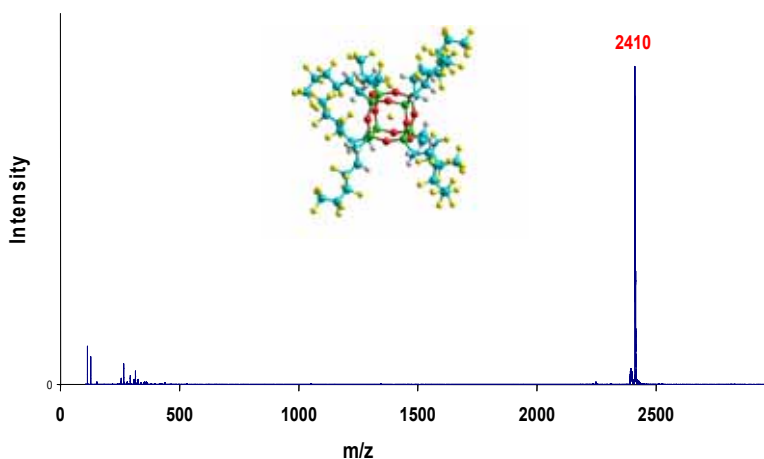
Figure 13. ESI mass spectrum of fluoride species derived from [(CF$_3$(CF$_2$)$_3$(CH$_2$)$_2$]$_8$T$_8$.

368 Å^2. These results contrast with a recent x-ray crystal structure[37b] that gives a calculated cross-section of 350 Å^2. The solid state structure, however, shows a highly ordered parallel arrangement of the fluorohexyl side chains such that each unit resembles a cylinder. This is presumably a solid state packing effect and contrasts with the globular structures predicted by our modeling of the isolated cage system.   The ordering in solids has been modeled successfully in long chain perfluoroalkanes and polytetrafluoroethylene, but only by using higher order terms in the molecular dynamics force fields in order to reproduce the observed helical chain structure.[76-78] The POSS cage with capping groups of a similar fluoroalkane, tridecafluorooctyl, did not yield a mass spectrum with

19

enough signal to obtain ion mobility measurements.

Conclusions

In summary, we have succeeded in observing a series of fluoridated POSS monomers with assorted capping R-groups. When synthesizing these species, it is essential to restrict the amount of water present to avoid hydrolysis of the cage and the resulting variety of products. The intact cages yield mass spectra in the negative ion ESI and/or the positive ion MALDI experiments. In negative ion ESI studies, the POSS monomer contains a fluoride ion in the center of the cage. DFT calculations show this to be energetically favorable, and the theoretical cross sections of the resulting species agree well with the cross sections of species seen in experiment. In the positive ion MALDI studies, the incorporated fluoride ion is protonated, yielding an HF molecule in the center, and a sodium ion is bound to the outside of the cage. This has also been shown to be energetically favorable, and again matches the experimental results. While binding of a lithium ion is more energetically favorable than binding of a sodium ion, the abundance of adventitious sodium ions present under the experimental conditions utilized results in a propensity to form the sodiated species.

The effectiveness of the synthesis of a fluoridated POSS molecule depends on the electronic properties of the capping groups. Each of the encapsulated F^- species seen in this study has electron-withdrawing capping groups that leave the center of the cage with a positive charge. This charge stabilizes the encapsulated fluoride structure and also leads to an effective mechanism for F^- insertion. If the capping groups are instead electron-donating, such as alkyl groups, the cage has a net negative charge and the fluoridated structure is destabilized. Attempts to encapsulate a fluoride in these cages failed, and reactions with TMAF resulted in no change to the starting structures.

Following the success of fluoridating POSS monomers, attempts are being made to react TMAF with a variety of POSS oligomers containing electron-withdrawing R-groups under strictly

anhydrous synthetic conditions in the hope that one or more cages will incorporate fluoride. Such species should show a strong negative ion ESI spectrum and analogous positive ion MALDI spectra. Incorporation of fluoride into these oligomers should increase the ionization efficiency of these molecules, resulting in stronger molecular ion peaks. It is our hope that this new technique will allow us to study a number of oligomers which have not been accessible in the past.

Supporting information available at

http://pubs3.acs.org/acs/journals/supporting_information.esi_volume_list?incoden=cmatex

FIGURE CAPTIONS

1. Synthesis and structure of $F^-@Ph_8T_8$.

2. ESI mass spectrum of oxo species derived from Ph_8T_8 and $Ph_{12}T_{12}$.

3. $Ph_7T_7O^-$, $Ph_9T_9O^-$ and $Ph_{11}T_{11}O^-$ structures derived from Ph_8T_8 and $Ph_{12}T_{12}$.

4. ESI mass spectrum of $F^-@Phenyl_8T_8$. The ^{13}C isotope distribution commencing with m/z = 1051 corresponds to the theoretically expected distribution.

5. MALDI mass spectrum and ATD of $HF@Phenyl_8T_8Na^+$.

6. ESI mass spectrum of fluoride species derived from Vi_8T_8, $Vi_{10}T_{10}$ and $Vi_{12}T_{12}$ mixture.

7. MP2 Stabilization Energies for V_8T_8 Fluoride Monomer Species.

8. MALDI mass spectrum and ATD of fluoride species derived from sodiated $HF@Styrenyl_8T_8$.

9. Structure of sodiated $HF@Styrenyl_8T_8$ ion. σ_{expt} = 321 Å^2 and σ_{calc}= 325 Å^2

10. ESI mass spectrum of fluoride species derived from $(i\text{-}Bu)_7(C_6H_5CH=CH_2)_8T_8$. Silicon scrambling has occurred.

11. (a) HOMO of $[(CF_3(CH_2)_2]_8T_8$ comprised of cage oxygen lone pairs.(b) LUMO of $[(CF_3(CH_2)_2]_8T_8$ comprised of cage oxygen antibonding $\sigma*$ orbitals. Frontier orbitals are primarily centered on R group.

12. Two-dimensional contour plots of the B3LYP/6-311++G(d,p) molecular electrostatic potentials of R_8T_8 POSS cages; R=CH_3, CF_3, $CHCH_2$. The plotting plane in panels a-c contains the center of the POSS cage and 4 oxygen atoms, while panels d-f show a diagonal plane through the center of the cage and 4 silicon atoms. The increment between adjacent contours is 2.5 kcal/mol-electron with positive and negative values shown in blue and red, respectively. In panels a-c and

d-f, the contours vary from -100.5 to +100.5 and from -80.5 to +80.5 kcal/mol-electron, respectively. The distance along each axis in plots a-c (d-f) is 12 (16) angstroms.

13. ESI mass spectrum of fluoride species derived from $[(CF_3(CF_2)_3(CH_2)_2]_8T_8$.

Table 1. Collision Cross-Sections (Å^2) of the negative POSS Fluoride Monomer Ions.

Species	Mass	X-ray[b] Cross-section	ESI Cross-section	Theory
$F^-@Ph_8T_8$	1051	260	268	260
$F^-@Vi_8T_8$	651	168	165	167
$F^-@Vi_{10}T_{10}$	809		189	190
$F^-@Vi_{12}T_{12}$	967		210	212,214[c]
$F^-@Sty_8T_8$	1259	343	346	343
$F^-@i\text{-}Bu_6Sty_2T_8$	985		258	258[d]
$F^-@i\text{-}Bu_5Sty_3T_8$	1032		272	271[d]
$F^-@i\text{-}Bu_4Sty_4T_8$	1076		283	284[d]
$F^-@Fpr_8T_8$	1211	261[a]	251	256
$F^-@Fhex_8T_8$	2411	350[a]	376	368

Vi = vinyl; Ph = phenyl; Sty = styrenyl; i-Bu = i-butyl; Fhex = $(CF_3)(CF_2)_3(CH_2)_2$;

Fpr = $CF_3CH_2CH_2$;

$T_8 = Si_8O_{12}$

a. Ref. 37

b. Calculated value for the neutral species.

c. Values correspond to two possible isomers.

d. Values identical for all possible isomers within experimental error.

Table 2. Collision Cross-Sections (Å^2) of the Sodiated POSS Fluoride Monomers.

Species	Mass	X-ray[a]	MALDI (Na$^+$) Cross-section	Theory (Na$^+$)
HF@ Sty$_8$T$_8$Na$^+$	1284		321	325
HF@Ph$_8$T$_8$Na$^+$	1075	263	254	257
HF@Vi$_8$T$_8$Na$^+$	674	168	165	167
HF@Fpr$_8$T$_8$Na$^+$	1235		218	216

Vi = vinyl; Ph = phenyl; Sty = styrenyl; i_Bu = i-butyl; Fpr = fluoropropyl; T$_8$ = Si$_8$O$_{12}$

a. calculated value for the neutral species.

Table 3. MP2 and DFT Stabilization Energies for POSS Fluoride Monomers.[a]

Species[b]	ΔE[c] B3LYP/ 6-31G*	ΔE[d] B3LYP/ 6-311++G(2df)	ΔE[e] MP2/6- 311++G(2df)
F$^-$@(CF$_3$)$_8$T$_8$ [f]	-170	-120	-270
fa-(CF$_3$)$_8$T$_8$F$^-$ [f]	-154	-102	-297
F$^-$@(CH$_3$)$_8$T$_8$ [f]	-112	-57	-70
F$^-$@Vi$_8$T$_8$ [f]	-119	-63	-77
fa-Vi$_8$T$_8$F$^-$ [f]	-80	-26	-37
HF@Vi$_8$T$_8$ [f]	+12	+29	+19
fa-Vi$_8$T$_8$HF$^+$ [f]	-22	-11	-11
HF@Vi$_8$T$_8$Na$^+$ [g]	-40	-15	-30[h]
HF@Vi$_8$T$_8$Li$^+$ [g]	-59	-32	-47[h]
[HF@Vi$_8$T$_8$]NaCl [i]	-8	15	40
[HF@Vi$_8$T$_8$]LiCl [i]	-12	12	-4
F$^-$@[CF$_3$CH$_2$)$_2$]$_8$T$_8$ [f]	-171		

Vi = vinyl; T$_8$ = Si$_8$O$_{12}$

a. All structures computed at the B3LYP/6-31G* level. All binding energies include B3LYP/6-31G* zero point vibrational energy corrections (scaled by 0.9806; see Scott, A.P., Radom, L. *J. Phys. Chem.* **1996,** *100,* 16502.)
b. All optimized structures have F$^-$ or HF body-centered unless specifically designated fa = "face".
c. B3LYP/6-31G*//B3LYP/6-31G* level of theory.
d. B3LYP/6-311++G(2df)//B3LYP/6-31G* level of theory.
e. MP2/6-311++G(2df)//B3LYP/6-31G* level of theory. Core orbitals were frozen in the MP2 calculation unless otherwise noted.
f. Binding energy ΔE = E(HF/F$^-$-POSS) - E(POSS) - E(HF/F$^-$).
g. Binding energy ΔE = E(HF-POSS-Li$^+$/Na$^+$) - E(POSS) - E(HF) – E(Li$^+$/Na$^+$).
h. Core orbitals were included in MP2 calculation.
i. Binding energy ΔE = E(HF-POSS-NaCl/LiCl) - E(POSS) - E(HF) – E(NaCl/LiCl).

Table 4. Neutral POSS Cluster Binding Energies (kcal/mol) as a Function of Cage Size.

Species[a,b]	LiCl	Li$_2$Cl$_2$	Li$_4$Cl$_4$	NaCl	Na$_2$Cl$_2$	Na$_4$Cl$_4$	KCl
T$_6$H$_6$	-42.7			-14.7			+35
T$_8$H$_8$	-13.5	-11.2	-10.0	-10.1	-7.9	-7.2	1.3
T$_{10}$H$_{10}$	-15.2			-9.7			+11.1

H = hydrogen; T$_8$ = Si$_8$O$_{12}$

a. Binding energy, $\Delta E = E(\text{neutral parent}) + E(X_nCl_n) - E(X_nCl_n \text{ cluster})$, where n = 1, 2 ,4

b. 6-311G* basis set with B3LYP functional; full energy minimization.

REFERENCES

1.   Voronkov, M.G. and Lavrentyev, V.I., *Polyhedral Oligosilsesquioxanes and Their Homo Derivatives.* Topics in Current Chemistry, 1982. **102**: p. 199-236.

2.   Agaskar, P.A., *New Synthetic Route to the Hydridospherosiloxanes Oh-H8si8o12 and D5h-H10si10o15.* Inorganic Chemistry, 1991. **30**(13): p. 2707-2708.

3.   Agaskar, P.A. and Klemperer, W.G., *The Higher Hydridospherosiloxanes - Synthesis and Structures of Hnsino1.5n (N=12, 14, 16, 18).* Inorganica Chimica Acta, 1995. **229**(1-2): p. 355-364.

4.   Baney, R.H., Itoh, M., Sakakibara, A., and Suzuki, T., *Silsesquioxanes.* Chemical Reviews, 1995. **95**(5): p. 1409-1430.

5.   Lichtenhan, J.D., *Polyhedral Oligomeric Silsesquioxanes - Building-Blocks for Silsesquioxane-Based Polymers and Hybrid Materials.* Comments on Inorganic Chemistry, 1995. **17**(2): p. 115-130.

6.   Lichtenhan, J.D., *Polymeric Materials Encyclopedia*, ed. J.C. Salamore. 1996: CRC Press, NY. 7769-7778.

7.   Li, G.Z., Wang, L.C., Ni, H.L., and Pittman, C.U., *Polyhedral oligomeric silsesquioxane (POSS) polymers and copolymers: A review.* Journal of Inorganic and Organometallic Polymers, 2001. **11**(3): p. 123-154.

8.   Phillips, S.H., Haddad, T.S., and Tomczak, S.J., *Developments in nanoscience: polyhedral silsesquioxane (POSS)-polymers oligomeric.* Current Opinion in Solid State & Materials Science, 2004. **8**(1): p. 21-29.

9.   Li, G.Z. and Pitman, C.U., *Macromolecules Containing Metals and Metal-like Elements*, A.S.C. Abd El Aziz, C.E.; Pittman, C.U; Zeldin, M., Editor. 2005, John Wiley & Sons: Hoboken, NJ. p. 79-131.

10.   Iacono, S.T., Budy, S.M., Mabry, J.M., and Smith, D.W., *Synthesis, Characterization, and Surface Morphology of Pendant Polyhedral Oligomeric Silsesquioxane Perfluorocyclobutyl Aryl Ether Copolymers.* Macromolecules, 2007.

11.   Koh, K., et al., *Precision synthesis of a fluorinated polyhedral oligomeric silsesquioxane-terminated polymer and surface characterization of its blend film with poly(methyl methacrylate).* Macromolecules, 2005. **38**(4): p. 1264-1270.

12.   Dodiuk, H., Rios, P.F., Dotan, A., and Kenig, S., *Hydrophobic and self-cleaning coatings.* Polymers for Advanced Technologies, 2007. **18**(9): p. 746-750.

13.   Tuteja, A., Choi, W., Ma, M.L., Mabry, J.M., Mazzella, S.A., Rutledge, G.C., McKinley, G.H., and Cohen, R.E., *Designing superoleophobic surfaces.* Science, 2007. **318**(5856): p. 1618-1622.

14.   Baker, E.S., Gidden, J., Fee, D.P., Kemper, P.R., Anderson, S.E., and Bowers, M.T., *3-Dimensional structural characterization of cationized polyhedral oligomeric silsesquioxanes (POSS) with styryl and phenylethyl capping agents.* International Journal of Mass Spectrometry, 2003. **227**(1): p. 205-216.

15.   Gidden, J., Kemper, P.R., Shammel, E., Fee, D.P., Anderson, S., and Bowers, M.T., *Application of ion mobility to the gas-phase conformational analysis of polyhedral oligomeric silsesquioxanes (POSS).* International Journal of Mass Spectrometry, 2003. **222**(1-3): p. 63-73.

16.   Baker, E.S., Gidden, J., Anderson, S.E., Haddad, T.S., and Bowers, M.T., *Isomeric structural characterization of polyhedral oligomeric silsesquioxanes (POSS) with styryl and epoxy phenyl capping agents.* Nano Letters, 2004. **4**(5): p. 779-785.

17.   Bowers, M.T., Kemper, P.R., von Helden, G., and van Koppen, P.A.M., *Gas-phase ion chromatography: Transition metal state selection and carbon cluster formation.* Science,

1993. **260**(5113): p. 1446-1451.

18.   von Helden, G., Hsu, M.-T., Kemper, P.R., and Bowers, M.T., *Structures of carbon cluster ions from 3 to 60 atoms: Linears to rings to fullerenes.* Journal of Chemical Physics, 1991. **95**(5): p. 3835-3837.

19.   Wyttenbach, T. and Bowers, M.T., *Gas-phase conformations: The ion mobility/ion chromatography method.* Topics in Current Chemistry, 2003. **225**: p. 207-232.

20.   Gidden, J., Jackson, A.T., Scrivens, J.H., and Bowers, M.T., *Gas phase conformations of synthetic polymers: Poly (methyl methacrylate) oligomers cationized by sodium ions.* International Journal of Mass Spectrometry, 1999. **188**(1-2): p. 121-130.

21.   Gidden, J., Wyttenbach, T., Batka, J.J., Weis, P., Jackson, A.T., Scrivens, J.H., and Bowers, M.T., *Folding energetics and dynamics of macromolecules in the gas phase: Alkali ion-cationized poly(ethylene terephthalate) oligomers.* Journal of the American Chemical Society, 1999. **121**(6): p. 1421-1422.

22.   Gidden, J., Bowers, M.T., Jackson, A.T., and Scrivens, J.H., *Gas-phase conformations of cationized poly(styrene) oligomers.* Journal of the American Society for Mass Spectrometry, 2002. **13**(5): p. 499-505.

23.   Gidden, J., Wyttenbach, T., Jackson, A.T., Scrivens, J.H., and Bowers, M.T., *Gas-phase conformations of synthetic polymers: Poly(ethylene glycol), poly(propylene glycol), and poly(tetramethylene glycol).* Journal of the American Chemical Society, 2000. **122**(19): p. 4692-4699.

24.   Baker, E.S., Bernstein, S.L., and Bowers, M.T., *Structural characterization of G-quadruplexes in deoxyguanosine clusters using ion mobility mass spectrometry.* Journal of the American Society for Mass Spectrometry, 2005. **16**(7): p. 989-997.

25.   Gabelica, V., Baker, E.S., Teulade-Fichou, M.P., De Pauw, E., and Bowers, M.T., *Stabilization and structure of telomeric and c-myc region intramolecular G-quadruplexes: The role of central cations and small planar ligands.* Journal of the American Chemical Society, 2007. **129**(4): p. 895-904.

26.   Baumketner, A., Bernstein, S.L., Wyttenbach, T., Bitan, G., Teplow, D.B., Bowers, M.T., and Shea, J.E., *Amyloid beta-protein monomer structure: A computational and experimental study.* Protein Science, 2006. **15**(3): p. 420-428.

27.   Wallace, W.E., Guttman, C.M., and Antonucci, J.M., *Molecular structure of silsesquioxanes determined by matrix-assisted laser desorption/ionization time-of-flight mass spectrometry.* Journal of the American Society for Mass Spectrometry, 1999. **10**(3): p. 224-230.

28.   Anderson, S.E., Baker, E.S., Mitchell, C., Haddad, T.S., and Bowers, M.T., *Structure of hybrid polyhedral oligomeric silsesquioxane propyl methacrylate oligomers using ion mobility mass spectrometry and molecular mechanics.* Chemistry of Materials, 2005. **17**(10): p. 2537-2545.

29.   Anderson, S.E., Mitchell, C., Haddad, T.S., Vij, A., Schwab, J.J., and Bowers, M.T., *Structural characterization of POSS siloxane dimer and trimer.* Chemistry of Materials, 2006. **18**(6): p. 1490-1497.

30.   Bassindale, A.R., Pourny, M., Taylor, P.G., Hursthouse, M.B., and Light, M.E., *Fluoride-ion encapsulation within a silsesquioxane cage.* Angewandte Chemie-International Edition, 2003. **42**(30): p. 3488-3490.

31.   Bassindale, A.R., Parker, D.J., Pourny, M., Taylor, P.G., Horton, P.N., and Hursthouse, M.B., *Fluoride ion entrapment in octasilsesquioxane cages as models for ion entrapment in zeolites. Further examples, X-ray crystal structure studies, and investigations into how and why they may be formed.* Organometallics, 2004. **23**(19): p. 4400-4405.

32.   Xiang, K.H., Pandey, R., Pernisz, U.C., and Freeman, C., *Theoretical study of structural and electronic properties of H-silsesquioxanes.* Journal of Physical Chemistry B, 1998. **102**(44): p. 8704-8711.

33.   Wichmann, D. and Jug, K., *MSINDO study of hydridosilsesquioxanes.* Journal of Physical

Chemistry B, 1999. **103**(46): p. 10087-10091.

34. Jug, K. and Wichmann, D., *MSINDO study of large silsesquioxanes.* Journal of Computational Chemistry, 2000. **21**(16): p. 1549-1553.

35. Franco, R., Kandalam, A.K., Pandey, R., and Pernisz, U.C., *Theoretical study of structural and electronic properties of methyl silsesquioxanes.* Journal of Physical Chemistry B, 2002. **106**(7): p. 1709-1713.

36. Poliskie, G.M., Haddad, T.S., Blanski, R.L., and Gleason, K.K., *Characterization of the phase transitions of ethyl substituted polyhedral oligomeric silsesquioxane.* Thermochimica Acta, 2005. **438**(1-2): p. 116-125.

37. (a) Iacono, S.T., Vij, A., Grabow, W., Smith, Jr., D. W., and Mabry, J.M., Chem. Commun., 2007, p. 4992–4994. (b) Mabry, J.M., Vij, A., Viers, B.D., Blanski, R.A., and Schlaefer, C.E., Angewandte Chemie-International Edition. **manuscript submitted for publication**.

38. Haddad, T.S., Viers, B.D., and Phillips, S.H., *Polyhedral oligomeric silsesquioxane (POSS)-styrene macromers.* Journal of Inorganic and Organometallic Polymers, 2001. **11**(3): p. 155-164.

39. Lichtenhan, J.D., Schwab, J.J., An, Y.-Z., Reinerth, W., Carr, M.J., Feher, F.J., Terroba, R., and Liu, Q. 2005: US Patent 06972312 B1.

40. Blanski, R.L., Phillips, S.H., and Lee, A., Polymer Preprints, 2001. **42**(1): p. 173-174.

41. Iacono, S.T., Vij, A., Grabow, W., Smith, J., D.W., and Mabry, J.M., *Facile synthesis of hydrophobic fluoroalkyl functionalized silsesquioxane nanostructures.* Chem. Commun., 2007(47): p. 4992-4994.

42. Pangborn, A.B., Giardello, M.A., Grubbs, R.H., Rosen, R.K., and Timmers, F.J., *Safe and convenient procedure for solvent purification.* Organometallics, 1996. **15**(5): p. 1518-1520.

43. Wyttenbach, T., Kemper, P.R., and Bowers, M.T., *Design of a new electrospray ion mobility mass spectrometer.* International Journal of Mass Spectrometry, 2001. **212**(1-3): p. 13-23.

44. Mason, E.A. and McDaniel, E.W., *Transport properties of ions in gases.* 1988, New York: Wiley. xvi, 560 p.

45. Case, D.A., Pearlman, D.A., Caldwell, J.W., Cheatham, T.E. III, Wang, J., Ross, W.S., Simmerling, C.L., Darden, T.A., Merz, K.M., Stanton, R.V., Cheng, A.L., Vincent, J.J., Crowley, M., Tsui, V., Gohlke, H., Radmer, R.J., Duan, Y., Pitera, J., Massova, I., Seibel, G.L., Singh, U.C., Weiner, P.K., and Kollman, P.A., *AMBER 7.* 2002, University of California, San Francisco.

46. Case, D.A., Darden, T.A., Cheatham, T.E. III, Simmerling, C.L., Wang, J., Duke, R.E., Luo, R., Merz, K.M., Wang, B., Pearlman, D.A., Crowley, M., Brozell, S., Tsui, V., Gohlke, H., Mongan, J., Hornak, V., Cui, G., Beroza, P., Schafmeister, C., Caldwell, J.W., Ross, W.S., and Kollman, P.A., *AMBER 8.* 2004, University of California, San Francisco.

47. Case, D.A., Pearlman, D.A., Caldwell, J.W., Cheatham, T.E. III, Ross, W.S., Simmerling, C., Darden, T., Merz, K.M., Stanton, R.V., Cheng, A., Vincent, J.J., Crowley, M., Tsui, V., Radmer, R., Duan, Y., Pitera, J., Massova, I., Seibel, G.L., Singh, U.C., Weiner, P., and Kollman, P.A., *AMBER 6.* 1999, University of California, San Francisco.

48. Sun, H., *Ab-Initio Calculations and Force-Field Development for Computer-Simulation of Polysilanes.* Macromolecules, 1995. **28**(3): p. 701-712.

49. Sun, H. and Rigby, D., *Polysiloxanes: Ab initio force field and structural, conformational and thermophysical properties.* Spectrochimica Acta Part a-Molecular and Biomolecular Spectroscopy, 1997. **53**(8): p. 1301-1323.

50. Itami, Y., Marciniec, B., and Kubicki, M., *Functionalization of octavinylsilsesquioxane by ruthenium-catalyzed silylative coupling versus cross-metathesis.* Chemistry-a European Journal, 2004. **10**(5): p. 1239-1248.

51. von Helden, G., Hsu, M.-T., Gotts, N., and Bowers, M.T., *Carbon cluster cations with up to 84 Atoms: Structures, formation mechanism, and reactivity.* Journal of Physical Chemistry, 1993. **97**(31): p. 8182-8192.

52.   von Helden, G., Wyttenbach, T., and Bowers, M.T., *Inclusion of a MALDI ion source in the ion chromatography technique: Conformational information on polymer and biomolecular ions.* International Journal of Mass Spectrometry and Ion Processes, 1995. **146**: p. 349-364.

53.   Mesleh, M.F., Hunter, J.M., Shvartsburg, A.A., Schatz, G.C., and Jarrold, M.F., *Structural information from ion mobility measurements: Effects of the long-range potential.* Journal of Physical Chemistry, 1996. **100**(40): p. 16082-16086.

54.   Shvartsburg, A.A. and Jarrold, M.F., *An exact hard-spheres scattering model for the mobilities of polyatomic ions.* Chemical Physics Letters, 1996. **261**(1-2): p. 86-91.

55.   Kohn, W., Becke, A.D., and Parr, R.G., *Density functional theory of electronic structure.* Journal of Physical Chemistry, 1996. **100**(31): p. 12974-12980.

56.   Stephens, P.J., Devlin, F.J., Chabalowski, C.F., and Frisch, M.J., *Ab-Initio Calculation of Vibrational Absorption and Circular-Dichroism Spectra Using Density-Functional Force-Fields.* Journal of Physical Chemistry, 1994. **98**(45): p. 11623-11627.

57.   Becke, A.D., *Density-Functional Thermochemistry .3. The Role of Exact Exchange.* Journal of Chemical Physics, 1993. **98**(7): p. 5648-5652.

58.   Becke, A.D., *Density-Functional Exchange-Energy Approximation with Correct Asymptotic-Behavior.* Physical Review A, 1988. **38**(6): p. 3098-3100.

59.   Ditchfield, R., Hehre, W.J., and Pople, J.A., *Self-Consistent Molecular-Orbital Methods .9. Extended Gaussian-Type Basis for Molecular-Orbital Studies of Organic Molecules.* Journal of Chemical Physics, 1971. **54**(2): p. 724-&.

60.   Hehre, W.J., Ditchfield, R., and Pople, J.A., *Self-Consistent Molecular-Orbital Methods .12. Further Extensions of Gaussian-Type Basis Sets for Use in Molecular-Orbital Studies of Organic-Molecules.* Journal of Chemical Physics, 1972. **56**(5): p. 2257-&.

61.   Dill, J.D. and Pople, J.A., *Self-Consistent Molecular-Orbital Methods .15. Extended Gaussian-Type Basis Sets for Lithium, Beryllium, and Boron.* Journal of Chemical Physics, 1975. **62**(7): p. 2921-2923.

62.   Francl, M.M., Pietro, W.J., Hehre, W.J., Binkley, J.S., Gordon, M.S., Defrees, D.J., and Pople, J.A., *Self-Consistent Molecular-Orbital Methods .23. A Polarization-Type Basis Set for 2nd-Row Elements.* Journal of Chemical Physics, 1982. **77**(7): p. 3654-3665.

63.   Harihara.Pc and Pople, J.A., *Influence of Polarization Functions on Molecular-Orbital Hydrogenation Energies.* Theoretica Chimica Acta, 1973. **28**(3): p. 213-222.

64.   Gordon, M.S., *The Isomers of Silacyclopropane.* Chemical Physics Letters, 1980. **76**(1): p. 163-168.

65.   Frisch, M.J., Trucks, G.W., Schlegel, H.B., Scuseria, G.E., Robb, M.A., Cheeseman, J.R., Montgomery, J., J. A., Vreven, T., Kudin, K.N., Burant, J.C., Millam, J.M., Iyengar, S.S., Tomasi, J., Barone, V., Mennucci, B., Cossi, M., Scalmani, G., Rega, N., Petersson, G.A., Nakatsuji, H., Hada, M., Ehara, M., Toyota, K., Fukuda, R., Hasegawa, J., Ishida, M., Nakajima, T., Honda, Y., Kitao, O., Nakai, H., Klene, M., Li, X., Knox, J.E., Hratchian, H.P., Cross, J.B., Bakken, V., Adamo, C., Jaramillo, J., Gomperts, R., Stratmann, R.E., Yazyev, O., Austin, A.J., Cammi, R., Pomelli, C., Ochterski, J.W., Ayala, P.Y., Morokuma, K., Voth, G.A., Salvador, P., Dannenberg, J.J., Zakrzewski, V.G., Dapprich, S., Daniels, A.D., Strain, M.C., Farkas, O., Malick, D.K., Rabuck, A.D., Raghavachari, K., Foresman, J.B., Ortiz, J.V., Cui, Q., Baboul, A.G., Clifford, S., Cioslowski, J., Stefanov, B.B., Liu, G., Liashenko, A., Piskorz, P., Komaromi, I., Martin, R.L., Fox, D.J., Keith, T., Al-Laham, M.A., Peng, C.Y., Nanayakkara, A., Challacombe, M., Gill, P.M.W., Johnson, B., Chen, W., Wong, M.W., Gonzalez, C., and Pople, J.A., *Gaussian 03, Revision C.02.* 2004, Gaussian, Inc.: Wallingford CT.

66.   Schmidt, M.W., Baldridge, K.K., Boatz, J.A., Elbert, S.T., Gordon, M.S., Jensen, J.H., Koseki, S., Matsunaga, N., Nguyen, K.A., Su, S.J., Windus, T.L., Dupuis, M., and Montgomery, J.A., *General Atomic and Molecular Electronic-Structure System.* Journal of Computational Chemistry, 1993. **14**(11): p. 1347-1363.

67.   Gordon, M.S. and Schmidt, M.W., *Theory and Applications of Computational Chemistry, the first forty years*, C.E. Dykstra, et al., Editors. 2005, Elsevier: Amsterdam.

68.   Krishnan, R., Binkley, J.S., Seeger, R., and Pople, J.A., *Self-Consistent Molecular-Orbital Methods .20. Basis Set for Correlated Wave-Functions.* Journal of Chemical Physics, 1980. **72**(1): p. 650-654.

69.   Clark, T., Chandrasekhar, J., Spitznagel, G.W., and Schleyer, P.V., *Efficient Diffuse Function-Augmented Basis-Sets for Anion Calculations .3. The 3-21+G Basis Set for 1st-Row Elements, Li-F.* Journal of Computational Chemistry, 1983. **4**(3): p. 294-301.

70.   Frisch, M.J., Pople, J.A., and Binkley, J.S., *Self-Consistent Molecular-Orbital Methods .25. Supplementary Functions for Gaussian-Basis Sets.* Journal of Chemical Physics, 1984. **80**(7): p. 3265-3269.

71.   Moller, C. and Plesset, M.S., *Note on an Approximation Treatment for Many-Electron Systems.* Physical Review, 1934. **46**(7): p. 618-622.

72.   Pople, J.A., Binkley, J.S., and Seeger, R., *Theoretical Models Incorporating Electron Correlation.* International Journal of Quantum Chemistry, 1976: p. 1-19.

73.   Frisch, M.J., Headgordon, M., and Pople, J.A., *A Direct Mp2 Gradient-Method.* Chemical Physics Letters, 1990. **166**(3): p. 275-280.

74.   Bartlett, R.J. and Silver, D.M. in *Int. J. Quantum Chem. Symp.* 1975.

75.   Kudo, T., Machida, K., and Gordon, M.S., *Exploring the mechanism for the synthesis of silsesquioxanes. 4. The synthesis of T-8.* Journal of Physical Chemistry A, 2005. **109**(24): p. 5424-5429.

76.   Holt, D.B. and Farmer, B.L., *Modeling of helix reversal defects in polytetrafluoroethylene I. Force field development and molecular mechanics calculations.* Polymer, 1999. **40**(16): p. 4667-4672.

77.   Holt, D.B. and Farmer, B.L., *Modeling of helix reversal defects in polytetrafluoroethylene II. Molecular dynamics simulations.* Polymer, 1999. **40**(16): p. 4673-4684.

78.   Borodin, O., Smith, G.D., and Bedrov, D., *A quantum chemistry based force field for perfluoroalkanes and poly(tetrafluoroethylene).* Journal of Physical Chemistry B, 2002. **106**(38): p. 9912-9922.

SUPPORTING INFORMATION AVAILABLE:

Table S1. ^{29}Si and ^{19}F NMR characterization of POSS syntheses.

Capping Ligand	^{29}Si (before)[a,c]	^{29}Si (after)[b,c]	^{19}F (before)[a,d]	^{19}F (after)[b,d]
vinyl	**-80.0**	**-83.0**	na	**-25.5**
phenyl	**-78.1**	**-80.7**	na	**-26.5**
styrenyl	**-78.2**	**-81.0**	na	**-24.5**
trifluoropropyl	**-66.7**	**-70.4**	-69.7	-28.7 -69.2
nonafluorohexyl	**-66.4**	**-70.1**	-82.4, -117.1, -125.2, -127.0	-28.7 -82.3, -117.1, -125.3, -127.0
tridecafluorooctyl	**-66.6**	**-70.7**	-82.1, -117.0, -122.7, -123.7, -124.3, -127.1	-28.8 -82.3, -117.2, -122.9, -123.8, -124.4, -127.3

a. NMR chemical shifts of POSS monomers before reaction with TMAF

b. NMR chemical shifts of POSS monomers after reaction with TMAF

c. Referenced to external tetramethylsilane at 0 ppm

d. Referenced to external CFCl$_3$ at 0 ppm